RECONSTRUCTING ORGAN VASCULATURE AND IDENTIFYING MORPHOLOGICAL CHANGES THROUGH THE UTILIZATION OF SEQUENTIAL BLOCK-FACE IMAGING BY MILLING WITH ULTRAVIOLET EXCITATION

by
Omar Abunofal

A thesis submitted to the Department of Biomedical Engineering
in partial fulfillment of the requirements for the degree of

Master of Sciences

in Biomedical Engineering

Chair of Committee: Chandra Mohan

Co-Chair of Committee: David Mayerich

Committee Member: Howard Gifford

University of Houston
December 2021

DEDICATION/EPIGRAPH

I dedicate my thesis work to my family who supported me and stood by me in every step and every way. I am forever thankful to their life-long support and for motivating me to enter this program.

ACKNOWLEDGMENTS

This work acknowledges Dr. Chandra Mohan for allowing me the opportunity to be a part of his laboratory during my undergraduate years and for helping gain research experience, which provided me a great stepping-stone for being in the master's program at the University of Houston and for conducting this thesis work. I express my sincere gratitude to Dr. Mohan for his patience, sharing his knowledge, and for being of help and support in every step and every way.

This work also acknowledges the great mentorship and guidance of Dr. David Mayerich for his assistance and making this collaborative work a success. I would also like to thank Dr. Mayerich's post-doctorate fellows, Dr. Jiaming Guo, Dr. Camille Arthur, and Dr. Pavel Govyadinov, for their great help and guidance during the thesis project.

I would like to thank Dr. Mohan's laboratory staff members and post-doctorate fellows, Kamala Vanarsa, Dr. Yong Du, Dr. Anto Sam Crosslee, and Yanping Chen, for assisting me every time I needed help with certain laboratory procedures and for aiding my thesis work by providing the biological samples I needed for my experiment. Additionally, I want to thank the academic advisor of the biomedical engineering department, Dr. Charlotte Waits, for her remarkable assistance and advisory over my master's journey.

Lastly, I acknowledge the outstanding efforts of the chairman of the biomedical engineering department, Dr. Metin Akay, for ensuring student success and setting a great graduate program that sets the graduates to a great start for their career journey.

ABSTRACT

Medical imaging is a significant medical procedure for diagnosing and characterizing various diseases. The gold standard in diagnosing diseases using medical imaging is imaging a stained tissue biopsy using standard staining procedures under light microscopy. Besides that, nuclear imaging modalities are commonly used for volumetric imaging, especially for internal organs. As a multitude of imaging modalities are emerging, various limitations within different imaging modalities remain existent. 2-dimensional (2D) imaging displays limited information to the pathologists due to the limited imaging depth. 3-dimensional (3D) imaging, namely nuclear imaging, presents several challenges in the medical field due to the minimal accessibility in medical facilities, expensive procurement costs, and challenges with data interpretation. In this work, we propose a novel imaging system that allows 3D imaging from 2D scans through a facile approach. The imaging system is based on the use of a motorized microtome for sectioning paraffin-embedded biological samples along with the use of UV light for stain excitation. Thus, we employ serial block-face imaging of paraffin-embedded biological samples from wild-type and systemic lupus erythematosus (SLE) mice that were intracardially perfused with India-ink for vascular staining. We were interested in reconstructing the vasculature of the mouse liver and creating 3D rendering models of the kidney glomeruli in order to observe the extent of SLE manifestation that our imaging system can aid in identifying. We designed a mold chamber that can be used for deep paraffin embedding since we aim to accomplish volumetric imaging of 3 mm to 1 cm depth. Following image stacking, we performed image alignment and vascular segmentation for the liver as part of the

image processing procedure. We conclude that our imaging system is a robust platform yet a simple and inexpensive modality for 3D imaging. More research is warranted to transfer our work and findings from qualitative to quantitative models for assessing various disease characteristics within biological organs. Moreover, automating the system to achieve user-friendliness and high throughput would be a groundbreaking achievement that can lead the way to the commercialization of the imaging system.

TABLE OF CONTENTS

LIST OF FIGURES

I. INTRODUCTION:

Pathological imaging is a vital assessment method for diagnosing and characterizing a particular disease. Current pathological imaging modalities entail 2D imaging as well as other 3D imaging modalities such as nuclear imaging. 2D histopathological slides are considered the gold standard in diagnosing numerous diseases [1]. As 2D imaging is commonly used in pathological research, it commonly lacks volumetric depth that can display complex anatomical features of a certain organ. Images like computed tomography (CT) and magnetic resonance imaging (MRI) may require expert interpretations due to the lack of details that are needed to establish a teaching point [2]. Moreover, 2D echocardiographic technologies for measuring the left ventricular ejection fraction have shown limited diagnostic accuracy [3].

3-dimensional imaging (3D) is an emerging imaging technique that is intended to provide more details and characteristics of an imaged specimens. 3D imaging is an effective method of assessing various phenotypic characteristics. Moreover, 3D imaging provides valuable information in terms of disease progression, morphological changes, and ultrastructural alterations. Importantly, 3D imaging aids in deciding a therapy or medication in a medical setting. Nuclear imaging modalities, like X-ray computed tomography (CT), positron emission tomography (PET), and magnetic resonance imaging (MRI), produce 2D images that are then reconstructed to 3D images [4]. CT imaging is a minimally invasive procedure where cross-sectional images of the body are produced using X-ray. Scans are taken in succession along the

axial plane, and sections are combined to generate an image, mainly for soft and hard tissues. MRI scanning works by receiving resonance signals from hydrogen nuclei, which images water in tissues. Applications of MRI include studying skeletal physiology and tumors. However, both MRI and CT technologies are known to be expensive to obtain and generally not available in medical centers, which indicates that they are difficult to procure. Also, CT scans create artifacts especially if the patient being examined has prosthetics, and CT data can be insufficient compared to other soft-tissue imaging techniques [5].

Systemic lupus erythematosus (SLE) is an autoimmune disease that is influenced by multiple factors including genetic, immunological, endocrine, and environmental factors. B and T cell activation along with cytokine release and complement activation leads to organ damage in SLE patients. Females are more prone to SLE than men with a female to male occurrence ratio of 9 to 1 [6]. Diagnosis of SLE in a timely manner remains a challenge in healthcare. However, the pathogenesis of SLE is being unveiled over time as extensive biomarker research is being undertaken to understand the underlying molecular mechanisms of SLE progression. For instance, the upregulated presence of mediators like inflammatory cells, cytokines, chemokines, and infiltrating immune cells suggest an eminent manifestation of lupus nephritis (LN). Moreover, the gold standard for LN diagnosis is a renal biopsy where a small part of the lesion is taken for examination [7].

It was identified that SLE has rare involvement in liver dysfunction due to abnormal plasma protein pattern. Liver dysfunction is not attributed as a main organ pathology in SLE; however, around 15%-60% of SLE patients are prone to developing

abnormal liver test in their lifetime. Liver complications as a result of SLE manifestations include lupus hepatitis and other autoimmune liver diseases. Commonly, liver dysfunction is due to multiple causes, which can be a pre-existing condition of alcoholic/non-alcoholic fatty liver disease or drug induced [8-9].

Clinical biopsies are possibly repetitive throughout the course of the disease, which causes discomfort to the patient. Also, in some cases it is infeasible to take a biopsy of other organs, like the brain or the spinal cord. Radiological assessment is also undertaken to monitor the disease in SLE patients. However, current radiological modalities demonstrated limitations as they do not screen for specific LN manifestations. Therefore, the need for an imaging modality that goes beyond the standard anatomical imaging protocols is in need [10].

In this work, we present the use of a novel imaging modality developed in our lab that leverages 3D reconstruction from formalin-fixed paraffin-embedded biological 2D sections. The system is called Milling with Ultraviolet Excitation (MUVE), and it requires the use of UV light to fluoresce the staining dye for better imaging resolution. The system requires the use of a motorized microtome in which paraffin-embedded biological samples are sectioned and the block-face of the sample is imaged.

There were former studies that focused on the use of serial block-face imaging on biological samples to examine the ultrastructural characteristics of various organs. Takaki et al. conducted a study concerning serial block-face imaging using scanning electron microscopy where they were able to reconstruct the podocyte cytoplasmic processes of the glomerular basement membrane (GBM) from a kidney biopsy from a

SLE patient. Through serial imaging and 3D reconstruction, they identified podocyte penetration into the glomerular basement membrane, which suggests a pathological feature that is not commonly known [11]. Randles et al. studied the ultrastructural alterations of the glomeruli in Alport syndrome using serial block-face scanning electron microscopy (SBF-SEM) [12]. Randles group were able to quantify the GBM thickness, foot processes number, podocyte invasion length into the GBM in Alport syndrome mouse model using SBF-SEM and 3D reconstruction. They concluded that visualizing the glomeruli through the utilization of SBF-SEM is enhanced, and SBF-SEM can identify pathological features that are uncommon.

Unlike the work that was previously done, our imaging system employs the application of UV light instead of SEM, which spares a lengthy procedure of using SEM. Moreover, the imaging platform that we have developed aids in 3D reconstruction that is sufficient to identify pathological features in SLE biological samples. In this work, we present the buildup of the MUVE platform and establish how our current platform achieves simplicity and user-friendliness. We also present preliminary data that was collected upon the buildup of the initial prototype. We discuss the animal protocol procedure, induction of SLE in mice, conduction of SBF imaging, and vasculature reconstruction.

II. MATERIALS AND METHODS:

Animal work:

All animals were housed and sheltered at the University of Houston animal facility and given the proper care. Four mice were used in the experimental part of this work: two male 9 months old C57B6 wild-type mice and two male 9 months old B6SLE1YAA homozygous strain mice. The mice were euthanized by CO_2 exposure followed by cervical dislocation. Perfusion was done using a fluid pump (Grothen, Masterflex) with a tunable flow rate. The first C57B6 mouse was perfused with 25 mL 1x PBS intracardially via a 27-gauge needle followed by 25 mL of India-ink at a flow rate of 5 mL/min. The second C57B6 mouse was perfused with 25 mL 1x PBS intracardially via a 27-gauge needle followed by 25 mL of India-ink at a flow rate of

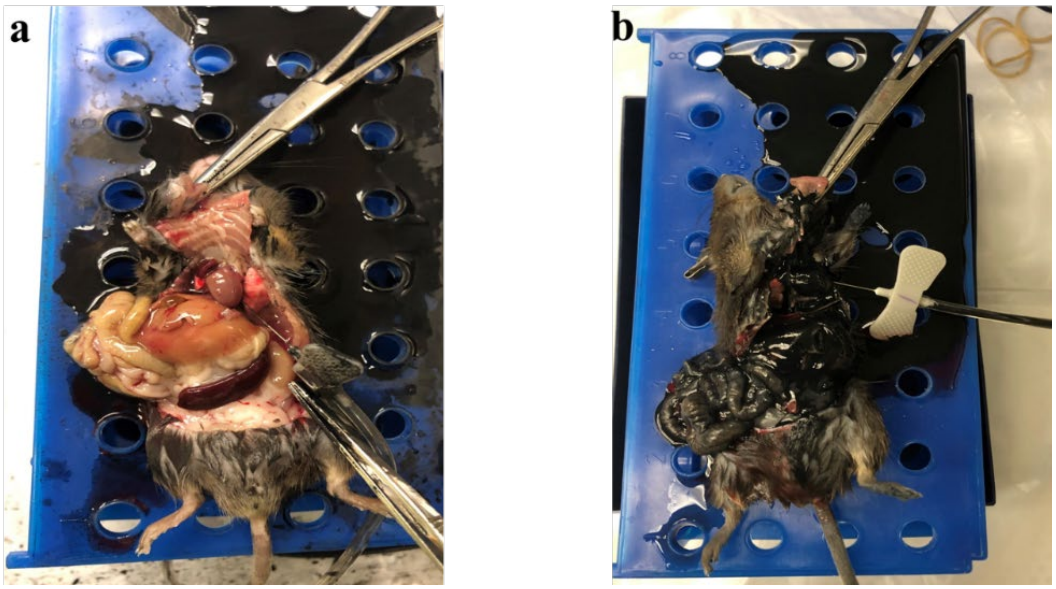

Figure 1. Intracardial mouse perfusion. **a)** Perfusion of 1x PBS intracardially via the left ventricle. Injecting PBS helps in flushing out the blood prior to India-ink perfusion. **b)** Perfusion of India-ink intracardially via the left ventricle using a 27-gauge needle.

10 mL/min. Both B6SLE1YAA mice were perfused with 45 mL 1x PBS intracardially via a 27-gauge needle followed by 45 mL of India-ink at a flow rate of 10 mL/min. Each mouse's liver was punctured to let the blood flush out as well as other fluids.

Figure 1 shows a mouse during PBS perfusion and India-in perfusion. As seen in figure 1b, the mouse's internal organs turn dark upon India-ink perfusion, which indicates that the vasculature is stained.

Paraffin-embedding process and the usage of the mold:

Each of the India-ink perfused organs, namely liver and kidneys, obtained from the WT and SLE mice were fixed in 10% formalin solution for 48 hours. Following fixation, the organs were dehydrated in 2 washes of each of 100%, 90%, 80%, and 70% ethanol for 1 hour in each wash. The biological samples were put in 3 washes of xylene for 1 hour in each wash to remove ethanol residue. Then, the biological samples were put in three washes of molten paraffin for 1 hour in each wash prior to the embedding process.

Deep paraffin embedding:

Since we are aiming to perform deep volumetric imaging of biological samples, the embedding orientation is set different from the traditional embedding orientation. As seen in figure b, the biological sample must be oriented vertically to achieve the maximal imaging depth. A 3D printed mold chamber was designed to aid

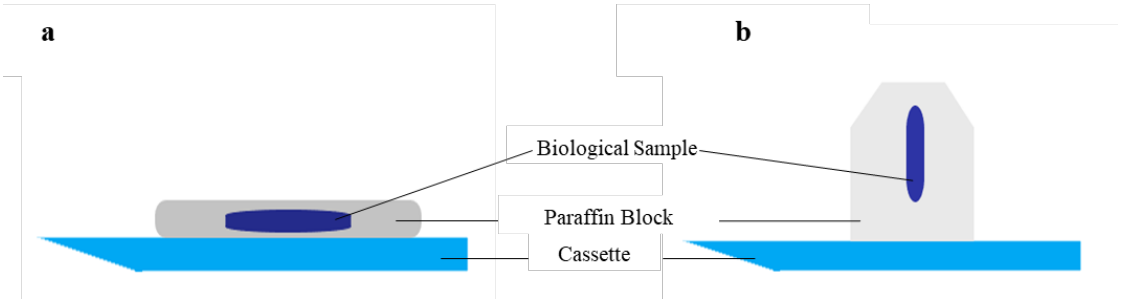

Figure 2. A comparison between traditional paraffin-embedding and deep-paraffin embedding. **a)** A schematic presentation of traditional paraffin-embedding where the biological sample is oriented horizontally. **b)** A schematic presentation of deep paraffin-embedding where the tissue sample is oriented vertically on order to achieve a maximal imaging depth.

in deep embedding as seen in figure 3. The mold chamber is used to hold the paraffin

mold in place to prevent the overflow of paraffin. Figure 4 demonstrates the deep-embedding process.

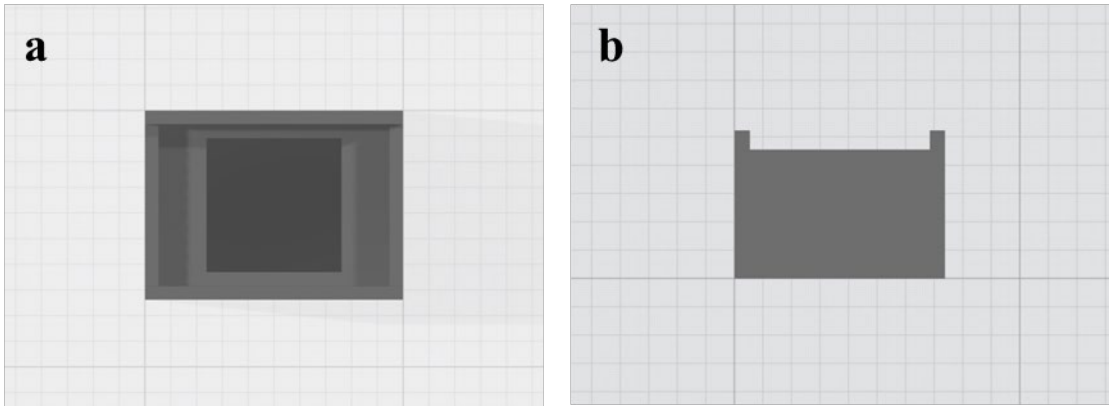

Figure 3. The mold chamber that is used for deep paraffin-embedding. **a)** Top view of the mold chamber. **b)** Front view of the mold chamber

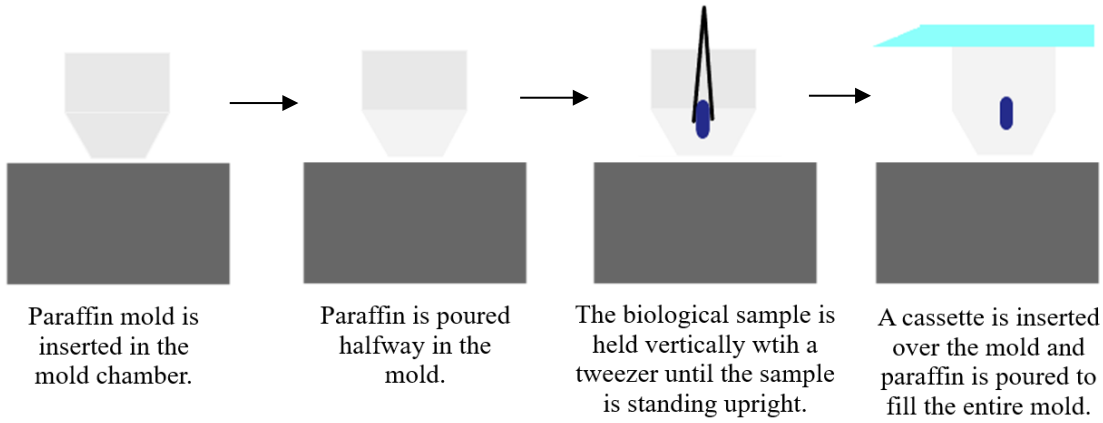

Figure 4. A schematic demonstration of the deep-embedding process using the mold chamber.

Buildup of MUVE:

The MUVE system shown in figure 5 is a rail-based platform where a rail poll (CEA1350, Thorlabs) is attached to a platform base. A vertical translator (CSN100, Thorlabs) is attached to the rail to allow linear, vertical translation of the objective. Another platform is inserted at the top of the rail where a 1X camera tube with C-mount (WFA4100, Thorlabs) is inserted on the platform with a Thorlab camera (Kiralux CS895CU, Thorlabs) attached to it. The C-mount of the vertical translator has a dichroic mirror (DFM1, Thorlabs) attached underneath it with a light reflector

attached underneath it. The use of the dichroic mirror is for filtering the UV light such that visible light can travel through the objective to the biological sample and UV light

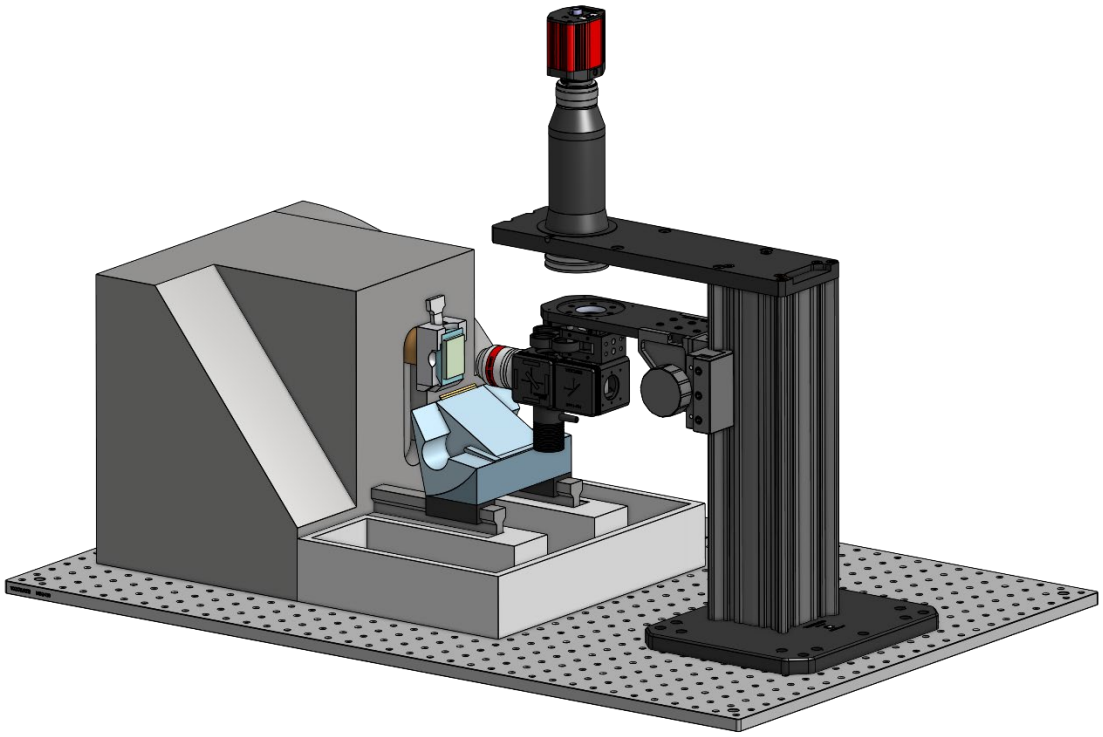

Figure 5. A computer-aided design of the rail-based MUVE platform imaging system with co-axial UV illumination.

can be reflected to the camera. A focusing knob along with a 10x objective (Nikon) are clamped to the C-mount of the reflector. A cage optical system containing 4 metal rods and 3 cage plates (CP02, Thorlabs) for the light path is also a part of the MUVE setup where the UV light source (M275L4, Thorlabs) is attached to the first cage plate and the other 2 cage plates with lenses are inserted in the metal rods for light focusing. Another UV light source amounts to the MUVE setup for a higher intensity illumination (FE200, Phoseon Technology) positioned at an oblique position with respect to the biological sample.

Serial block-face imaging:

Serial block-face imaging (SBF) is performed with the use of a motorized microtome (MICROM HM 355S, Thermo Scientific), which allows sectioning paraffin-embedded biological samples at various sectioning thicknesses ranging from 0.5 – 100 µm. SBF imaging is done by focusing the MUVE objective at a certain region of interest (ROI) of a biological sample, capturing an image via Thorcam, and taking a section of a specific thickness. This process is done sequentially for a desired sectioning depth.

Image alignment:

Images from the same stack were aligned by using an image alignment algorithm that was pre-written using a Python script. The algorithm works by taking the first image

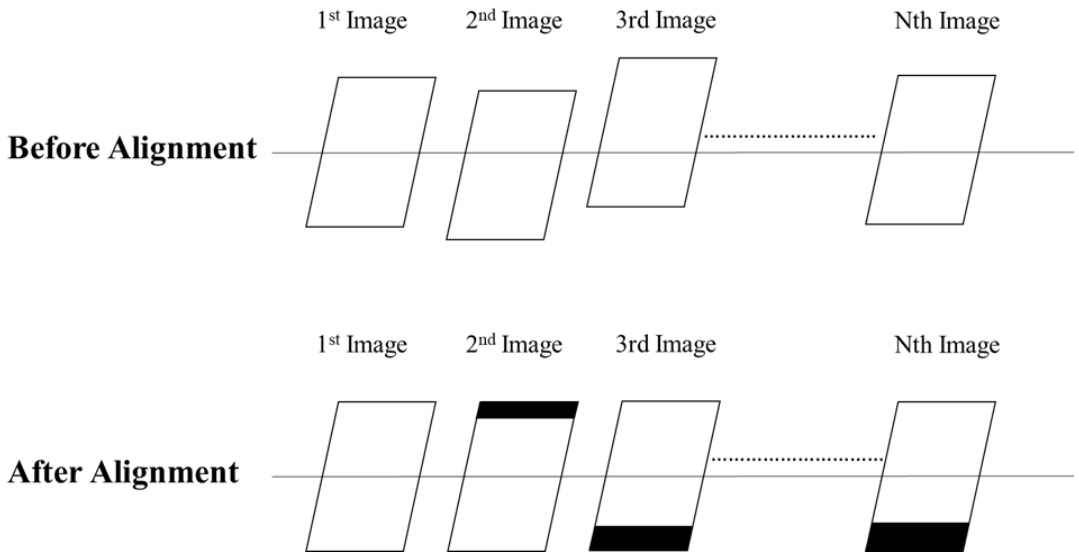

Figure 6. A schematic of image alignment. The top figure displays a series of images in an unaligned fashion, which represent the raw data. The bottom image shows the series of images after alignment by using the image alignment algorithm.

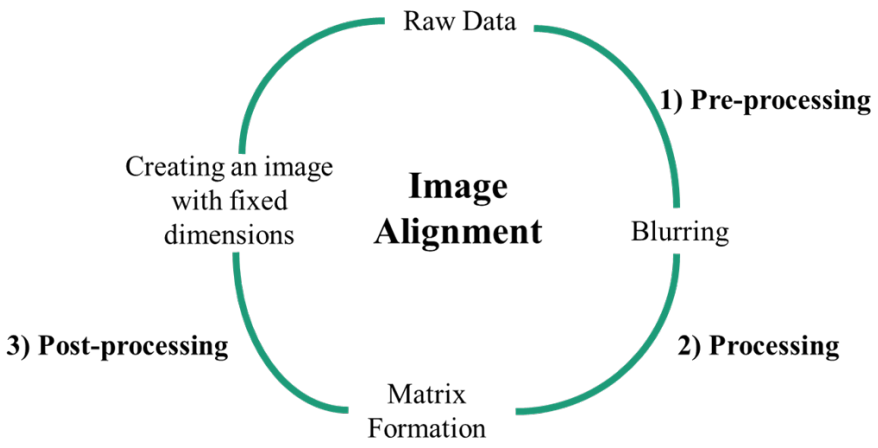

Figure 7. A diagram detailing the image alignment procedure.

and aligning to the next image and do so for the entire image stack, as illustrated in figure 6. The algorithm aligns the images by recognizing a unique pattern between each image. Additionally, the algorithm employs a metric called Enhanced Correlation Coefficient (ECC) that is supported by OpenCV in Python. ECC aids in estimating parameters of the motion model. As shown in figure 7, the alignment is done in 3 different steps: pre-processing, processing, and post-processing. During the pre-processing step, all the images from the raw data are blurred. Following the blurring process (processing step), a matrix is created for the first image. Then, a matrix is created for the second image, and the matrices of the second and first image are added. The matrices of all the images are added and the ECC is computed in order to identify a pattern between each image. Lastly, images with fixed dimensions are created during the post-processing step.

Segmentation:

Segmentation is a process done through programming via Python where the vasculature is extracted from the raw data of the images and presented in a 3D view. The method that is employed in this process is known as the minimum intensity

projection. Given that the vasculature is stained with India-ink, the dark parts of the images represent the vascular network. First, the image set is converted to gray scale 8 bits images. Then, the images are aggregated into 16x16x16 μm voxel cubes. The segmentation is done by setting a threshold. If a pixel intensity at any given position in an image is below the threshold, then the system will output a value of 0 for that pixel. Otherwise, the system will output a value of 1. All pixels with a value of 0 are extracted, and the 3D vasculature of the image set is viewed via Paraview software using the volume view option.

III. RESULTS:

Presentation of preliminary data:

This section presents images that were acquired using the MUVE platform upon the completion of its assembly. Evidently, the MUVE system can help with identifying various tissue properties. Figure 8 shows an India-ink perfused mouse kidney imaged via MUVE. We can observe the main characteristics that make up the

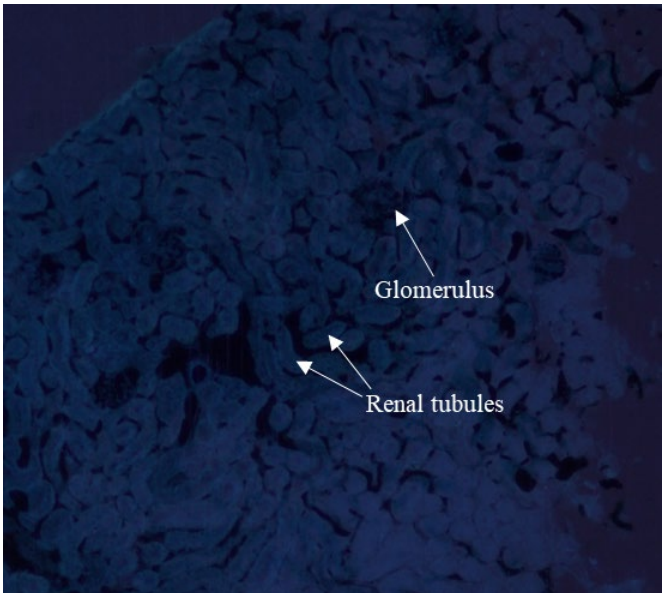

Figure 8. India-ink perfused wild type mouse kidney imaged with a 10X objective.

kidney in that figure. Namely, the India-ink perfusion into the organ vasculature is what outlines the tissue morphology and characteristics. Hence, we did not use any

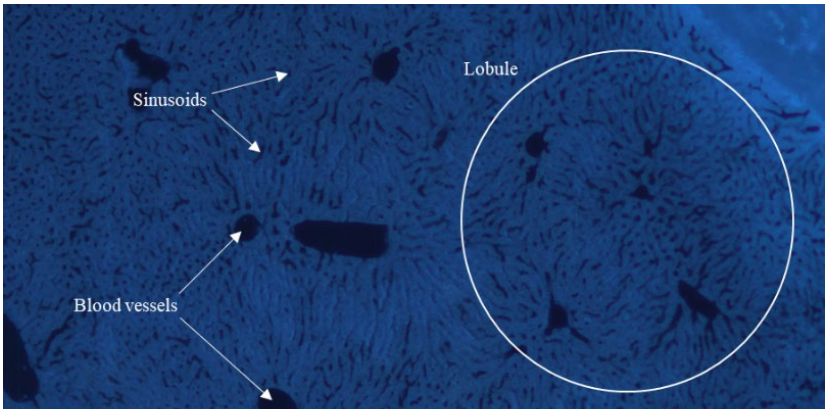

Figure 9. Liver sample imaged with a 10X objective. India-ink perfusion labels sinusoids and helps in differentiating blood vessels from other vascular components as well as tracing hepatic lobules.

other staining media in this work as we are only interested in studying the vasculature of the organs through India-ink perfusion. We can realize in figure 8 that the tortoise structure represents the renal tubules, and the cabbage-like circles represent the glomeruli.

Illumination (Oblique vs co-axial illumination):

The initial prototype of the MUVE platform consisted of a UV light source (M275L4, Thorlabs) that emitted UV at an output power range of 45-80 mW. The UV light source was inserted at a co-axial position relative to the biological sample. The illumination produced from the UV source mandates setting the exposure time at 950 ms. Therefore, the imaging process takes a longer time, and the image brightness appeared dimmer. To mitigate this issue, we utilized a Phoseon light source (FE 200,

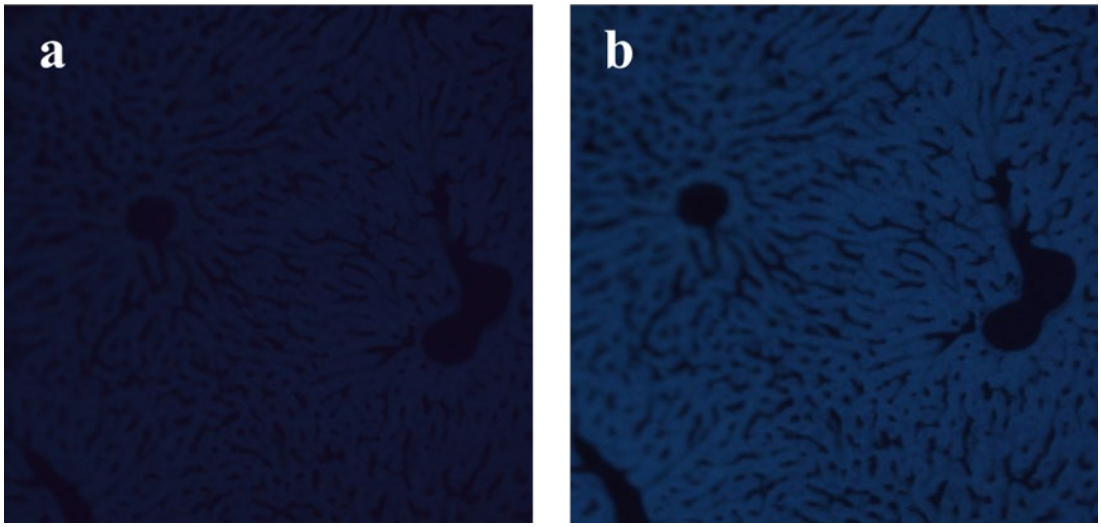

Figure 10. An India-ink perfused liver sample imaged with a 10x refractive objective. **a)** Co-axial UV illumination. **b)** Oblique UV illumination from a Phoseon UV lamp. Both images are from the same block-face but with different UV illumination sources.

Phoseon Technology) with an output power of 3 W. This light source allowed using an exposure time of 100 ms, which therefore allowed faster imaging process. At a 950 ms exposure time, we were capable to capture 5 total images per minute. However, at 100

ms exposure time, we were capable to capture 20 total images per minute, thus increasing the system's throughput by 4 times.

WT vs SLE liver and kidney block-face comparison:

As a part of the validation procedure, we were able to identify the morphological alterations between the WT and SLE liver and kidney by examining the block-face at different regions of interest (ROI) through the MUVE system.

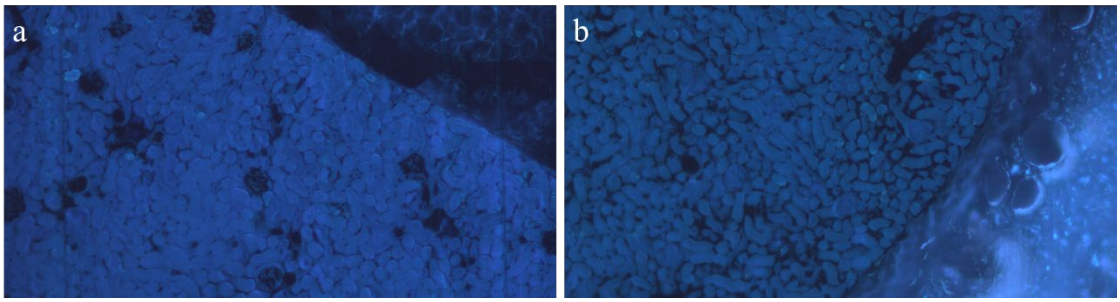

Figure 11. WT vs SLE India-ink-stained mouse kidney imaged via 10x objective. a) WT kidney, b) SLE kidney

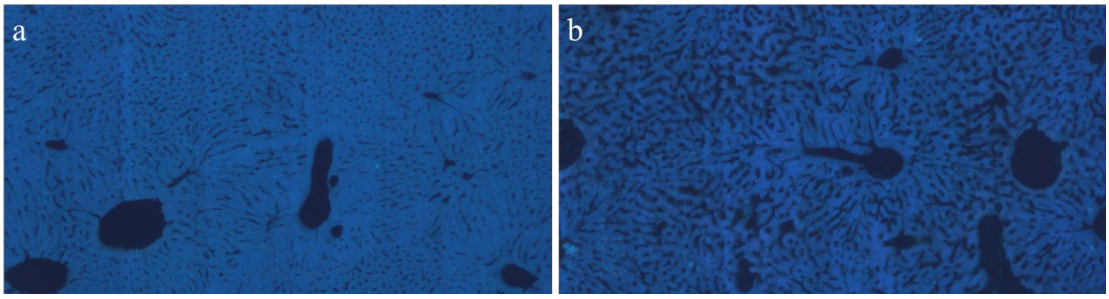

Figure 12. WT vs SLE India-ink-stained mouse liver image via 10x objective. a) WT liver, b) SLE liver

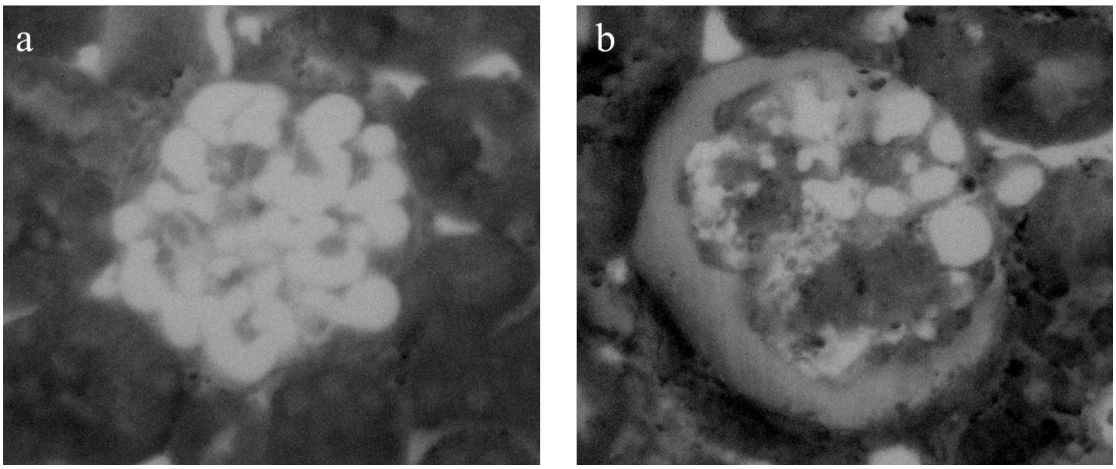

Figure 13. WT vs SLE kidney glomeruli imaged via 40x objective (ROI 1). a) WT glomerulus, b) SLE glomerulus

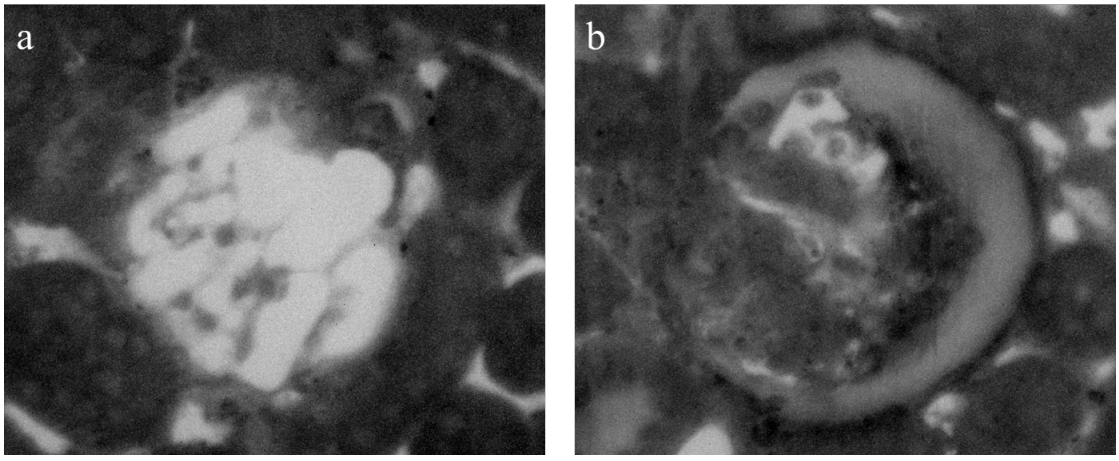

Figure 14. WT vs SLE kidney glomeruli imaged via 40x objective (ROI 2). a) WT glomerulus, b) SLE glomerulus

Figure 11 shows a comparison between a WT and SLE mouse kidney. SLE kidney shows a wider inter-tubular space. In figure 12, we can notice a higher sinusoidal density of SLE as compared to WT. That indicates a swollen liver vasculature as a result of SLE manifestation. Swollen vasculature can be attributed to hepatomegaly as observed by Imran et al. in a study that focused on analyzing the liver activities in SLE patients [13]. Glomerular crescent is a common manifestation LN that is observed in the kidney glomeruli. Glomerular crescents are formed due to excessive collagen and fibrin deposition along with parietal epithelial cells residing

along the circumference of the Bowman ’s capsule [14]. Figures 13 and 14 show examples of glomerular crescent formation due to lupus nephritis manifestation. Using SBF imaging via MUVE, we are able to observe the progression of the crescentic morphology along different depths by forming an AVI video (data not shown). This to further verify and characterize the extent of the disease progression.

Oscillation along the vertical axis:

The stacking size and sectioning process have impacted the image alignment by causing the paraffin cassette to oscillate along the vertical and horizontal axes over the process of SBF imaging. Oscillation has a direct impact on the image alignment process because with an increased stacking size the offset between consecutive images increases causing a reduced field of view. We postulated that the sectioning thickness or the stacking size might contribute to the offset after aligning an image stack. Thus, in order to confirm if the oscillatory effects are due to the sectioning thickness or the stacking size, we performed two different experiments. In the first experiment, we collected three stacks of images from paraffin-embedded liver sample where the stacking size was the same for all three, but the thickness was different resulting in different imaging volume: 150 images at 1 μm per section, 2 μm per section, and 3 μm per section. In the second experiment, we also collected three different stacks of images from paraffin-embedded kidney sample where the stacking size was different, but the imaging depth was the same. We conclude from those experiments that if we need to perform deep, volumetric imaging that requires a heavy stacking size (> 0.5 mm), then sectioning at 3 μm would be an ideal option. This is because at 3 μm we can achieve our desired imaging depth with a less stacking size; thus, the offset can be

minimized. However, if we need to perform volumetric imaging of less than 0.5 mm, then sectioning at 1 μm would be ideal because we would have a sufficient stacking size and the offset accumulation would not significantly affect the field of view of an image. Figure 15 shows how the offset is created between two consecutive sections after alignment. Figure 16 shows how the offset increases as we obtain more sections resulting in a decreased field of view as shown in the blank spaces along the bottom and the right margins of figure 16b. We must note that for the majority of our experiments in this study, we sectioned at 2 μm. The reason is because sectioning at 2 μm has caused minimal oscillatory effects. Aside from that, sectioning at 2 μm does not significantly ablate crucial anatomical features of a biological sample, namely liver, compared to sectioning at 3 μm. This will result in a more reliable segmentation result that closely resembles the actual vasculature of the liver. As shown in figure 17, sectioning at 1 μm does not significantly remove crucial layers. However, observing the changes between figures 18a and 18b inside the boxed regions, we can realize a significant vascular ablation between both frames, which can potentially affect the segmentation process as the segmented vasculature would not precisely resemble the

actual vasculature of the liver due to the heavy vascular ablation that is caused by sectioning at 3 μm.

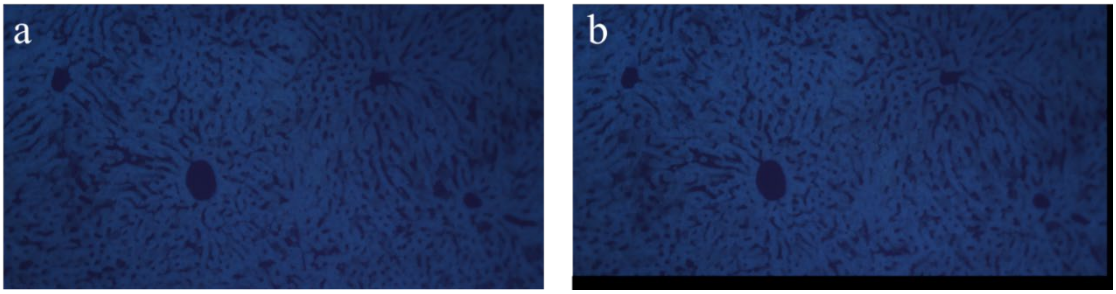

Figure 16. India-ink perfused liver imaged at 10x objective. Both images were captured consecutively. a) A capture of the first block-face. b) A capture of the second block-face. The sectioning thickness that was used is 2 μm. The black spaces that are found along the bottom and right margins in figure b are due to the offset that is created after aligning the images.

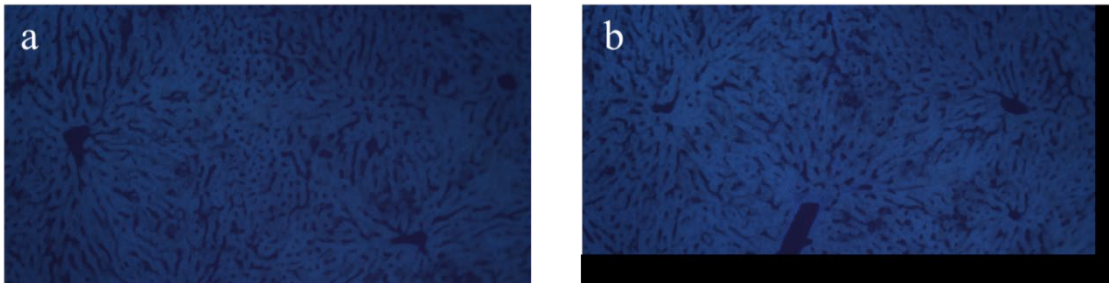

Figure 15. India-ink perfused liver imaged at 10x objective. a) A capture of the first block-face. b) A capture of the 49th block-face. Those two images show how the oscillation of the imaging system cause an accumulated offset after aligning the images.

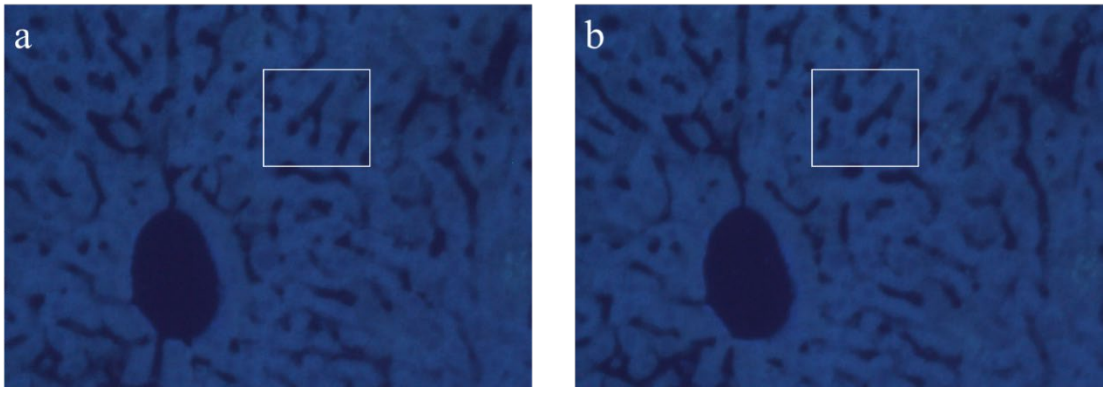

Figure 17. Sectioning at 1 μm. Figure b is the block-face that was revealed after sectioning the block-face that is shown in figure a

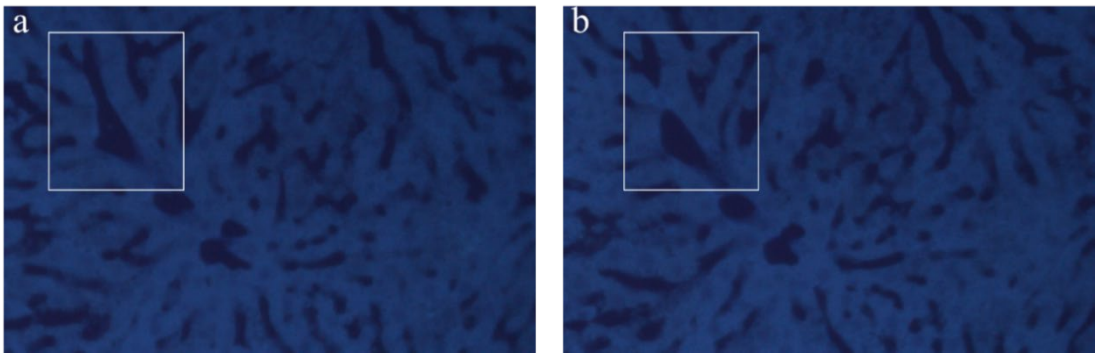

Figure 18. Sectioning at 3 µm. Figure b is the block-face that was revealed after sectioning the block-face that is shown in figure a

Liver segmentation:

Two stacks of images from WT and SLE liver were collected: 1296 images from WT liver, and 1500 images from SLE liver. All sections were 2 µm thick. Figure 15 shows the segmentation results where the vascular network of the liver is clearly shown. Figure 16 shows the segmentation results of SLE liver. It is clearly shown in this figure how the liver vasculature is swollen in comparison to its WT counterpart in

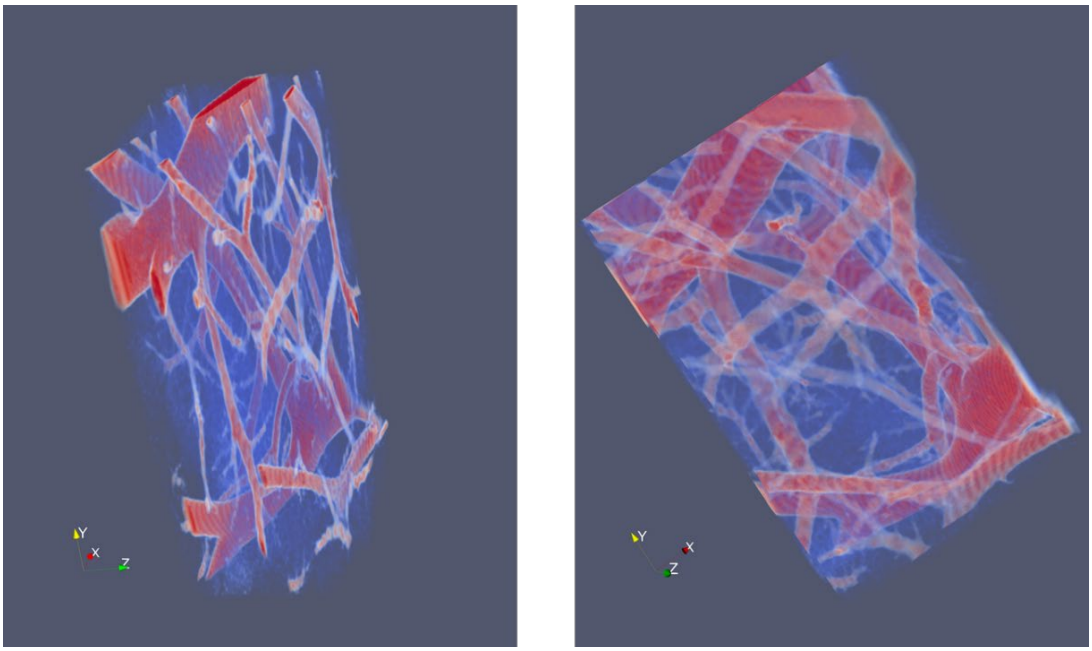

Figure 19. WT liver segmentation results.

figure 15. Consistent to the results shown in figure 12, segmenting the liver

vasculature can enable us to compare healthy liver and diseased liver vasculature by observing the vascularization pattern between both types. Figure 20 clearly shows a higher sinusoidal density as compared to figure 19.

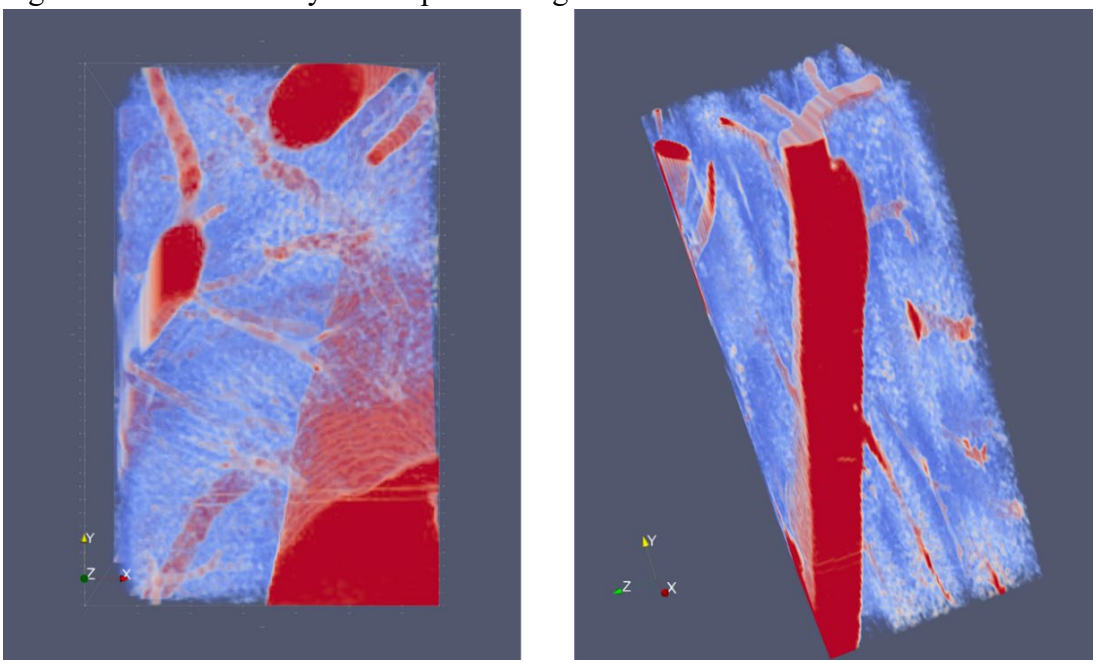

Figure 20. SLE liver segmentation results.

IV. DISCUSSION:

In this work, we have designed an imaging system that allows 3D imaging by reconstructing a stack of 2D scans using paraffin-embedded biological samples. The MUVE system operates with the use of a motorized microtome to collect the 2D scans. Our current results hold a great promise for the MUVE system as a potential 3D imaging device for biological samples. Moreover, the MUVE system has shown to establish a high level of versatility such that we can use the MUVE system to image the block-face of a paraffin-block simply and instantaneously to generally view the morphology of an organ. In this work, we carried out SBF imaging using India-ink perfused mouse organs. We reconstructed the liver vasculature from WT and SLE mice and identified major morphological differences. We were also interested in examining the kidney glomeruli of both samples where we created AVI models of the glomeruli of both WT and SLE mice (data not shown). We were able to identify common morphological features in SLE glomeruli in our work such that the MUVE platform can aid in identifying abnormal characteristics in kidney glomeruli such as glomerular crescent. We believe that by being able to have a visual representation of a biological sample at different depths, we can identify where exactly abnormal features starts to manifest, which highlights the robustness of 3D imaging.

To the best of our knowledge, there are no former studies that focused on reconstructing the liver vasculature of SLE mouse model. Our current results indicate that lupus hepatitis as a result of SLE can lead to ultra-vascularization in the liver as a result of hepatomegaly. The reconstructed SLE liver vasculature in figure 20 shows a significantly higher sinusoidal density as compared to figure 19, which can indicate a

sign of SLE manifestation. Concomitantly, using the MUVE system, we were able to identify the glomerular crescent structure, which is a common feature in LN.

While we were interested in reconstructing the organ vasculature in this work using our MUVE system, we must mention that the MUVE system can also be useful for reconstructing images of organs that are stained differently. If we are interested in nuclear staining, we can use the MUVE system to image organs that are stained with hematoxylin and eosin, HOECHST, or DAPI staining media. Moreover, we can use staining media that detects the presence of certain protein markers if we were interested in having a 3D visual representation to visualize the infiltration extent of those markers using the MUVE system.

As we establish the robustness of our imaging platform, we must acknowledge the limitations that are associated with our study. Firstly, the oscillatory effects that are exhibited due to the microtome blade force against the paraffin block creates an offset that is undesirable to the user as features within the biological samples are removed. We postulate that a possible way to minimize this issue is by having a more stable stage that is oriented differently. Secondly, our experiments were done on a very small sample size. We need to validate our results and findings by carrying out those experiments on a larger sample size to achieve consistency. Thirdly, this study lacks the use of numerical and statistical models that can better govern our results. As a future insight, we plan on performing statistical analysis for comparing certain liver and kidney features between WT and SLE mice. The metrics that we would be interested in observing are as follows: the ratio of the size glomerular capillaries to the glomerular space, cell detection and quantification around the glomerular space, the

distance between the Bowman's capsule and the podocytes, the quantification of the vascular density in the liver, and the quantification of the vessels' diameter in the liver. Undergoing statistical analysis to govern the findings of the mentioned metrics, we can better assess the disease progression using SBF imaging. We also aim to acquire a higher imaging depth in our future experiments in order to be able to visualize more features in an organ. For example, by having a deeper volumetric imaging of SLE liver, we can determine if the sinusoidal density would be consistent across different depths or not. Lastly, our current MUVE system design is operated manually, which can be time consuming and labor costly. By automating the MUVE system, we can achieve a significantly higher throughput and user-friendliness.

V. CONCLUSION:

In conclusion, SBF imaging via MUVE is a robust 3D imaging method that we have designed, fabricated, and developed using an inexpensive and simple approach. With the current results that we have attained using the MUVE system, we assert that our imaging system can be taken in various directions in research, such as image processing, pathology research, and deep volumetric imaging. By using the MUVE system, we believe that many questions and cues can be answered in the areas of biology and pathology.

REFERENCES

1. Gurcan MN, Boucheron LE, Can A, Madabhushi A, Rajpoot NM, Yener B. "Histopathological image analysis: a review." IEEE Rev Biomed Eng. 2009;2:147-71. doi: 10.1109/RBME.2009.2034865. Epub 2009 Oct 30. PMID: 20671804; PMCID: PMC2910932.
2. Ballantyne L. "Comparing 2D and 3D imaging." J Vis Commun Med. 2011 Sep;34(3):138-41. doi: 10.3109/17453054.2011.605057. PMID: 22023011.
3. Seraphim A, Westwood M, Bhuva AN, Crake T, Moon JC, Menezes LJ, Lloyd G, Ghosh AK, Slater S, Oakervee H, Manisty CH. "Advanced Imaging Modalities to Monitor for Cardiotoxicity." Curr Treat Options Oncol. 2019 Aug 8;20(9):73. doi: 10.1007/s11864-019-0672-z. PMID: 31396720; PMCID: PMC6687672.
4. Farahani N, Braun A, Jutt D, Huffman T, Reder N, Liu Z, Yagi Y, Pantanowitz L. "Three-dimensional Imaging and Scanning: Current and Future Applications for Pathology." J Pathol Inform. 2017 Sep 7;8:36. doi: 10.4103/jpi.jpi_32_17. PMID: 28966836; PMCID: PMC5609355.
5. Karatas OH, Toy E. "Three-dimensional imaging techniques: A literature review." Eur J Dent. 2014 Jan;8(1):132-140. doi: 10.4103/1305-7456.126269. PMID: 24966761; PMCID: PMC4054026.
6. Justiz Vaillant AA, Goyal A, Bansal P, Varacallo M. "Systemic Lupus Erythematosus." 2021 Aug 11. In: StatPearls [Internet]. Treasure Island (FL): StatPearls Publishing; 2021 Jan–. PMID: 30571026.

7. Schwartz N, Goilav B, Putterman C. “The pathogenesis, diagnosis and treatment of lupus nephritis.” Curr Opin Rheumatol. 2014 Sep;26(5):502-9. doi: 10.1097/BOR.0000000000000089. PMID: 25014039; PMCID: PMC4221732.
8. Chowdhary VR, Crowson CS, Poterucha JJ, Moder KG. “Liver involvement in systemic lupus erythematosus: case review of 40 patients.” J Rheumatol. 2008 Nov;35(11):2159-64. doi: 10.3899/jrheum.080336. Epub 2008 Sep 15. PMID: 18793002.
9. Shizuma, T. (2015). *Liver Complications Associated with Systemic Lupus Erythematosus.*
10. Thurman JM, Serkova NJ. “Non-invasive imaging to monitor lupus nephritis and neuropsychiatric systemic lupus erythematosus.” F1000Res. 2015 Jun 16;4:153. doi: 10.12688/f1000research.6587.2. PMID: 26309728; PMCID: PMC4536614.
11. Takaki T, Ohno N, Saitoh S, Nagai M, Joh K. “Podocyte penetration of the glomerular basement membrane to contact on the mesangial cell at the lesion of mesangial interposition in lupus nephritis: a three-dimensional analysis by serial block-face scanning electron microscopy.” Clin Exp Nephrol. 2019 Jun;23(6):773-781. doi: 10.1007/s10157-019-01701-0. Epub 2019 Feb 8. PMID: 30734164.
12. Randles M, Collinson S, Starborg T, Mironov A, Krendel M, Konigshausen E, Sellin L, Roberts Ian, Kadler K, Miner Jeffrey, Lennon R. “Three-dimensional

electron microscopy reveals the evolution of glomerular barrier injury." Sci Rep 6, 35068 (2016). https://doi.org/10.1038/srep35068

13. Imran S, Thabah MM, Azharudeen M, Ramesh A, Bobby Z, Negi VS. "Liver Abnormalities in Systemic Lupus Erythematosus: A Prospective Observational Study." Cureus. 2021 Jun 16;13(6):e15691. doi: 10.7759/cureus.15691. PMID: 34277279; PMCID: PMC8284411.
14. Anguiano L, Kain R, Anders HJ. "The glomerular crescent: triggers, evolution, resolution, and implications for therapy." Curr Opin Nephrol Hypertens. 2020 May;29(3):302-309. doi: 10.1097/MNH.0000000000000596. PMID: 32132388; PMCID: PMC7170443.